Colloids and Surfaces B: Biointerfaces 86 (2011) 370–377

Contents lists available at ScienceDirect

Colloids and Surfaces B: Biointerfaces

journal homepage: www.elsevier.com/locate/colsurfb

Solving EDL configuration near a dissimilarly charged protrusions surface model using perturbation method

Sung-Hwa Lin[a,*], Jyh-Ping Hsu[b], Shiojenn Tseng[c], Yung-Chih Kuo[d], Bo-Tau Liu[e]

[a] Department of Chemical and Materials Engineering, National Ilan University, No. 1, Sec. 1, Shennong Rd., Yilan City, Yilan County 26047, Taiwan, ROC
[b] Department of Chemical Engineering, National Taiwan University, No. 1, Sec. 4, Roosevelt Rd., Taipei City 10617, Taiwan, ROC
[c] Department of Mathematics, Tamkang University, No. 151, Yingzhuan Rd., Danshui Township, Taipei County 25137, Taiwan, ROC
[d] Department of Chemical Engineering, National Chung Cheng University, No. 168, University Rd., Minhsiung Township, Chiayi County 62102, Taiwan, ROC
[e] Department of Chemical and Materials Engineering, National Yunlin University of Science and Technology, No. 123, Sec. 3, University Rd., Douliou City, Yunlin County 64002, Taiwan, ROC

ARTICLE INFO

Article history:
Received 3 April 2011
Received in revised form 9 April 2011
Accepted 14 April 2011
Available online 21 April 2011

Keywords:
Dissimilarly charged protrusions (DCP)
Arbitrary surface morphology
Arbitrary surface charged condition
Fourier series
Perturbation method

ABSTRACT

In this work, an elementary, novel dissimilarly charged protrusions (DCP) surface model in an electrolyte solution considering simultaneously the complexity of both surface morphology and surface charged condition, which are concerned frequently on a biological cell membrane, on a modified micro-particle surface, or in a lab-on-a-chip biosensor device, is proposed. Based on Fourier series and the perturbation technique, the configuration of electrical double layer (EDL) near this complicated charged surface model is successfully solved semi-analytically. The numerical calculation reveals that, the methodology suggested in present study could deal with charged surface systems of arbitrary geography and of arbitrary charge distribution. In the analysis, three special subjects are discussed, including an isolated dissimilarly charged protrusion, the effect of protrusions, and the effect of dissimilarly charged condition on protrusions.

1. Introduction

A charged surface with arbitrary shape of protrusions, which might carry different kinds of charges from that on the rest domain of charged surface, are deeply concerned in fields of biological cell membrane and micro- or nano-scale modern, advanced technologies. For example: in therapeutics, DNA-loaded cationic lipid particles introduced for gene delivery in the cancer curing [1]; in biomedical engineering, the heparin-loaded cationic lipid particles applied in the differentiation of stem cells [2]; in drug delivery system, poly(acrylic acid)-grafted silica particle as an selective-filter functionalized drug delivery device [3]; in medicine, γ-MPS modified silica particle for the fabrication of dental nanocomposite [4]; in water treatment, the polymer-encapsulated silica particle, SG-PS-azo-IM particle for the adsorption of transition metal ions from the treated water [5]; and so forth. In preparing the micro- or nano-scale functionalized colloidal particles in these examples mentioned above, the surface on particles might possesses regions of different surface charge density, due to the association of external polymer chains, and moreover, the polymer protrusions appear on it, and correspondingly the surface morphology changes. Generally, the association efficiency of polymer chains on these colloidal particles plays a key step for their functions, and more often than not, the association efficiency (or loading efficiency) needs the capillary electrophoresis analysis. Consequently, understanding the charged condition on the surface of particles via solving the electrical double layer (EDL) configuration seems to be requisite. For a biological cell, based on the model set up since 1960s and called the fluid-mosaic model [6], the cell membrane (plasma membrane) is mainly composed of lipid bilayer and membrane proteins. The lipid bilayer is a lamella of two molecular monolayers, of which the molecules include phospholipids, phosphoacylglycerol and sphingomyelin, and glycolipids, cerebroside and ganglioside. The globular, granular membrane proteins are associated with the lipid bilayer via mainly the noncovalent interactions, i.e. both the hydrophilic and the hydrophobic forces. They may just contact with the hydrophilic planes through their polar amino acid side chains (called surface membrane proteins), or they may be embedded into the hydrophobic interior part of bilayer through their nonpolar amino acid side chains, leaving their hydrophilic ends outside the bilayer (called integral membrane proteins), or even, they may traverse the entire lipid bilayer. Typically, the thickness of lipid bilayer is about 50 Å (5 nm), and the complete width of lipid–protein bilayer matrix is about 80 Å (8 nm). There are over ten kinds of membrane proteins distributed randomly on lipid bilayer, and the molecular weights of them

* Corresponding author. Tel.: +886 39357400x701; fax: +886 39357025.
E-mail address: shlin@niu.edu.tw (S.-H. Lin).

0927-7765/$ – see front matter © 2011 Elsevier B.V. All rights reserved.
doi:10.1016/j.colsurfb.2011.04.023

Nomenclature

c_i^0	concentration of i-th ion species in the bulk solution
$c_{i,j}$	coefficient of j-th eigenfunction for i-th order term ψ_i
F	Faraday constant
$f_p(X)$	shape function of protrusion
$f_s(X)$	shape function of charged surface system
$h_s(x)$	height function of charged surface system
$H_S(X)$	$\kappa h_s(x)$
I	ionic strength of electrolyte solution
l_x	period of charged surface system
L_x	κl_x
n	total number of ion species
$\underline{n_s}$	unit normal vector of charged surface (outward)
R	gas constant
T	temperature
x	axis of Cartesian coordinate
X	κx
x_p	length of protrusion base
X_p	κx_p
y	axis of Cartesian coordinate
Y	κy
z	axis of Cartesian coordinate
Z	κz
z_i	valence of i-th ion species

Greek letters

ε	small perturbation parameter
ε_{es}	permittivity of electrolyte solution
κ	Debye–Huckel parameter
σ_f	surface charge density on flat surface
Σ_f	$\sigma_f/2IF\kappa^{-1}$
σ_p	surface charge density on protrusion
Σ_p	$\sigma_p/2IF\kappa^{-1}$
$\sigma_s(x)$	surface charge density on charged surface system
$\Sigma_s(X)$	$\sigma_s(x)/2IF\kappa^{-1}$
ϕ	electrical potential field
ψ	$F\phi/RT$
ψ_i	i-th order term for ψ

range approximately from 35,000 to 260,000 g/mol. The electron microscopic image of a fracture through the freeze-etching human erythrocyte membrane shows that, there are about 6.2×10^5 particles of 8.5 nm in diameter, responsible for about 20% of its surface area, and which are supposed to be two kinds of glocoproteins, i.e. sialoglycoprotein and some undetermined glycoprotein of 100,000 daltons, traversing through the entire lipid bilayer [7]. The charged condition on cell membrane is quite complicated. Four types of lipids and the membrane proteins may carry charges of different kinds. Via microelectrophoresis chamber of millimeters in diameter in electrophoresis, Seaman and his coworkers [8–10] found that, the charge density on the membrane of a human erythrocyte cell is of the order of 10^{-2} C/m^2, and which is mainly attributed to sialic acid ($pK_a = 2.6$) and some undetermined, bound carboxylic acid ($pK_a = 3.35$). In addition to both surface morphology and surface charged condition for cell membrane, the contact angle between the membrane protein and the lipid bilayer also increases the complexity in mathematical modeling [11]. Hence, in view of these, in the capillary electrophoresis, frequently used in the analysis of cell membrane, understanding both the surface morphology and the charged condition on membrane via solving EDL configuration seems also to be requisite.

Usually for mathematical modeling, the associated (loaded) polymer chains on a colloidal particle are considered as a soft layer [12,13], wherein, the polymer chains are taken as a homogeneous charged layer. For mathematical calculation, this may be fruitful, however more or less, some realistic conditions may become ambiguous, depending on the distribution of loaded polymer chains on the surface of particle. Limited works in the literature discuss the arbitrary surface morphology on the colloidal particle, not to mention the heterogeneous distribution of surface charges. Little works analyze the effect of irregular surface morphology on the colloidal particle based on Deryaguin approximation [14] or Fourier series [15–18], and the analyses reveal that little surface roughness or undulation may lead to significant variation in EDL configuration. The numerical result from a previous work [19] also shows that, slight undulation of a charged surface may result in a significant variation of fluid velocity near the surface. Therefore, to deal with both the complexity of surface morphology and charged condition, an attempt is made in this work to solve EDL configuration near a charged surface system possessing simultaneously the arbitrary geography and the arbitrary charge distribution. And for this, a dissimilar charged protrusions (DCP) surface model in an electrolyte solution, which gives consideration to complexity of these two in mathematical modeling, is suggested. The solution for this elementary, novel model based on Fourier series is introduced, and the discussion is confined to the condition of little surface roughness or protrusion, wherein the perturbation technique is applied.

2. Mathematical modeling

The dissimilarly charged protrusions surface model under consideration, which is immersed in an electrolyte solution, is illustrated in Fig. 1(a). This charged surface model is a one-dimensional, infinite, periodic, charged surface, wherein within each period of charged surface system, there are two distinct regions, including the dissimilarly charged protrusion, of which the surface charge density is σ_p, and the flat surface, of which the surface charge density is σ_f. Assuming that the height of charged surface system varies periodically along the abscissa, it can be described within a period by a piecewise-defined function as

$$H_s(X) = \varepsilon f_s(X) \tag{1}$$

$$f_s(X) = \begin{cases} f_p(X), X \in [-X_p/2, X_p/2] \\ 0, X \in [-L_x/2, -X_p/2) \text{ and } (X_p/2, L_x/2] \end{cases} \tag{2}$$

In these equations above and in Fig. 1(a), the lengths are scaled by Debye length, κ^{-1}, and they are $X = \kappa x$, $Y = \kappa y$, $Z = \kappa z$, $X_p = \kappa x_p$, $L_x = \kappa l_x$, and $H_s(X) = \kappa h_s(x)$, where x, y, z are the axes of Cartesian coordinate, x_p and l_x denote respectively the length of protrusion base and the period of charged surface system, $h_s(x)$ is the height function of charged surface system, and ε denotes a small perturbation parameter. The Debye–Huckel parameter κ is defined as $(2IF^2/\varepsilon_{es}RT)^{1/2}$, where I, F, R, T, and ε_{es} are the ionic strength of electrolyte solution, the Faraday constant, the gas constant, the temperature, and the permittivity of electrolyte solution, respectively, and the ionic strength of electrolyte solution is defined by $I = \sum_{i=1}^{n} z_i^2 c_i^0/2$, with z_i, c_i^0, and n being the valence of i-th ion species, the concentration of i-th ion species in the bulk solution, and the total number of ion species, respectively. For mathematical convenience, in each period of charged surface system, we consider the condition of symmetric geometry, and the origin has been chosen as the symmetric center, as this figure shows. In present study, we discuss the condition of little surface protrusion, therefore the height function of charged surface system is assumed the form as Eq. (1), a shape function $f_s(X)$ multiplied by the perturbation parameter, wherein the piecewise-defined function $f_s(X)$ is defined by $f_p(X)$ (the shape

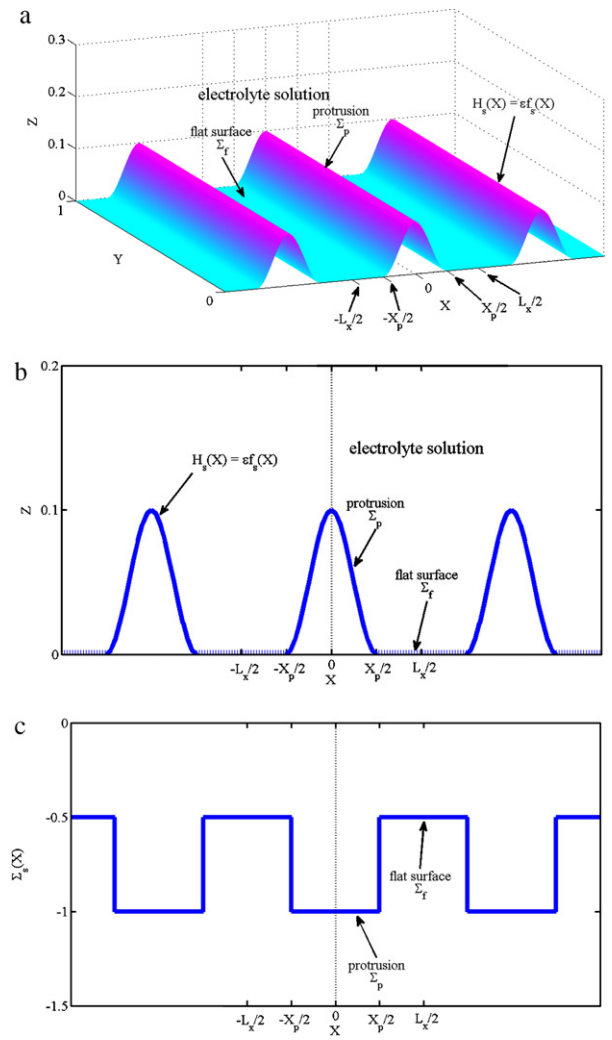

Fig. 1. (a) Schematic representation for the dissimilarly charged protrusions surface model in an electrolyte solution under consideration. (b) Lateral view for the charged surface model, where the solid curves and the dot lines denote the protrusions with surface charge density Σ_p, and the flat surfaces with surface charge density Σ_f, respectively. (c) Charged condition of the charged surface model, $\Sigma_s(X)$.

function of protrusion) in the region of protrusion, and 0 in the region of flat surface, respectively. The lateral view of charged surface system is shown in Fig. 1(b). The surface charge density $\sigma_s(x)$ on our charged surface can also be described within a period by a piecewise-defined function as

$$\Sigma_s(X) = \begin{cases} \Sigma_p, X \in [-X_p/2, X_p/2] \\ \Sigma_f, X \in [-L_x/2, -X_p/2) \text{ and } (X_p/2, L_x/2] \end{cases} \quad (3)$$

where the dimensionless terms are defined by $\Sigma_s(X) = \sigma_s(x)/2IF\kappa^{-1}$, $\Sigma_p = \sigma_p/2IF\kappa^{-1}$, and $\Sigma_f = \sigma_f/2IF\kappa^{-1}$, respectively. Fig. 1(c) illustrates the function $\Sigma_s(X)$. Based on both the values of X_p and L_x, the charged surface model such defined similar to Eqs. (1)–(3) is capable of simulating a charged surface composed of arbitrary geography and charged condition, and which will be discussed in Section 4. Under Debye–Huckel approximation, the linearized Poisson–Boltzmann equation in electrolyte solution can be expressed as follows:

$$\frac{\partial^2\psi}{\partial X^2} + \frac{\partial^2\psi}{\partial Z^2} - \psi = 0 \quad (4)$$

where $\psi = F\phi/RT$, with ϕ being the electrical potential field of EDL. The associated boundary conditions for Eq. (4) could be summarized as the following:

$$\left.\frac{\partial\psi}{\partial X}\right|_{X=0} = \left.\frac{\partial\psi}{\partial X}\right|_{X=L_x/2} = 0 \quad (5)$$

$$\varepsilon_{es}(-\nabla\phi)\big|_{z=h_s(x)}\underline{n}_s(x) = \sigma_s(x), \text{ or}$$

$$-\varepsilon\frac{df_s(X)}{dX}\left.\frac{\partial\psi}{\partial X}\right|_{Z=H_s(X)} + \left.\frac{\partial\psi}{\partial Z}\right|_{Z=H_s(X)} + \left[\varepsilon^2\left(\frac{df_s(X)}{dX}\right)^2 + 1\right]^{1/2}\Sigma_s(X) = 0 \quad (6)$$

$$\lim_{Z\to\infty}\psi = 0 \quad (7)$$

where $\underline{n}_s$ is the unit normal vector of charged surface (outward), and according to Eq. (1), it can be expressed as

$$\underline{n}_s = \frac{\langle -\varepsilon df_s(X)/dX, 0, 1\rangle}{[\varepsilon^2(df_s(X)/dX)^2 + 1]^{1/2}} \quad (8)$$

In these boundary conditions, i.e. Eqs. (5)–(7), Eq. (5) describes the symmetry of charged surface system at both $X=0$ and $X=L_x/2$, Eq. (6) implies the continuity of the normal component of displacement field across the charged surface, where we have assumed that there is no electrical field in the region under the charged surface for mathematical simplicity, and Eq. (7) implies the vanishment of electrical potential field at infinity.For the solution of electrical potential field, we express it as an asymptote expansion series with respect to ε:

$$\psi(X,Z) = \sum_{i=0}^{\infty}\varepsilon^i\psi_i(X,Z) \quad (9)$$

where $\psi_i(X,Z)$ denotes the i-th order term for $\psi(X,Z)$. Substitution of the equation above into Eq. (4) leads to

$$\sum_{i=0}^{\infty}\varepsilon^i\left(\frac{\partial^2\psi_i}{\partial X^2} + \frac{\partial^2\psi_i}{\partial Z^2} - \psi_i\right) = 0 \quad (10)$$

Setting the coefficients of terms of each order in the equation above equal to zero, and with the aid of Eqs. (5) and (7), the terms of each order for $\psi(X,Z)$ could be expressed by the eigenfunction expansions as

$$\psi_i(X,Z) = \sum_{j=0}^{\infty}c_{i,j}\cos\left(\frac{2\pi jX}{L_x}\right)e^{-(1+4\pi^2j^2/L_x^2)^{1/2}Z} \quad (11)$$

where $c_{i,j}$ means the coefficient of j-th eigenfunction for the i-th order term $\psi_i(X,Z)$, and which needs to be determined by Eq. (6) with the aid of orthogonality of Fourier cosine series. The boundary condition on the charged surface, expressed by Eq. (6), is an irregular boundary condition, therefore before applying Eq. (6), some terms in this equation need to be expanded as asymptote expansion series, and they are

$$\left.\frac{\partial\psi}{\partial X}\right|_{Z=H_s(X)} = \left.\frac{\partial\psi}{\partial X}\right|_{Z=0} + \left.\frac{\partial^2\psi}{\partial Z\partial X}\right|_{Z=0}\varepsilon f_s(X) + O(\varepsilon^2) \quad (12)$$

$$\left.\frac{\partial\psi}{\partial Z}\right|_{Z=H_s(X)} = \left.\frac{\partial\psi}{\partial Z}\right|_{Z=0} + \left.\frac{\partial^2\psi}{\partial Z^2}\right|_{Z=0}\varepsilon f_s(X) + \frac{1}{2}\left.\frac{\partial^3\psi}{\partial Z^3}\right|_{Z=0}\varepsilon^2 f_s^2(X) + O(\varepsilon^3) \quad (13)$$

$$\left[\varepsilon^2\left(\frac{\mathrm{d}f_s(X)}{\mathrm{d}X}\right)^2+1\right]^{1/2}=1+\frac{1}{2}\varepsilon^2\left(\frac{\mathrm{d}f_s(X)}{\mathrm{d}X}\right)^2+O(\varepsilon^4) \tag{14}$$

By substitution of these expansion series above into Eq. (6), we have after rearrangement

$$\left(\left.\frac{\partial\psi_0}{\partial Z}\right|_{Z=0}+\Sigma_s(X)\right)+\varepsilon\left(-\frac{\mathrm{d}f_s(X)}{\mathrm{d}X}\left.\frac{\partial\psi_0}{\partial X}\right|_{Z=0}+\left.\frac{\partial\psi_1}{\partial Z}\right|_{Z=0}+f_s(X)\left.\frac{\partial^2\psi_0}{\partial Z^2}\right|_{Z=0}\right)+\varepsilon^2\left[-\frac{\mathrm{d}f_s(X)}{\mathrm{d}X}\left.\frac{\partial\psi_1}{\partial X}\right|_{Z=0}-f_s(X)\frac{\mathrm{d}f_s(X)}{\mathrm{d}X}\left.\frac{\partial^2\psi_0}{\partial Z\partial X}\right|_{Z=0}+\left.\frac{\partial\psi_2}{\partial Z}\right|_{Z=0}+f_s(X)\left.\frac{\partial^2\psi_1}{\partial Z^2}\right|_{Z=0}+\frac{1}{2}f_s^2(X)\left.\frac{\partial^3\psi_0}{\partial Z^3}\right|_{Z=0}+\frac{1}{2}\left(\frac{\mathrm{d}f_s(X)}{\mathrm{d}X}\right)^2\Sigma_s(X)\right]+O(\varepsilon^3)=0 \tag{15}$$

Setting the coefficients of terms of each order in this equation above equal to zero, we arrive at the following identities:

$$\left.\frac{\partial\psi_0}{\partial Z}\right|_{Z=0}=-\Sigma_s(X) \tag{16}$$

$$\left.\frac{\partial\psi_1}{\partial Z}\right|_{Z=0}=\frac{\mathrm{d}f_s(X)}{\mathrm{d}X}\left.\frac{\partial\psi_0}{\partial X}\right|_{Z=0}-f_s(X)\left.\frac{\partial^2\psi_0}{\partial Z^2}\right|_{Z=0} \tag{17}$$

$$\left.\frac{\partial\psi_2}{\partial Z}\right|_{Z=0}=\frac{\mathrm{d}f_s(X)}{\mathrm{d}X}\left.\frac{\partial\psi_1}{\partial X}\right|_{Z=0}+f_s(X)\frac{df_s(X)}{dX}\left.\frac{\partial^2\psi_0}{\partial Z\partial X}\right|_{Z=0}-f_s(X)\left.\frac{\partial^2\psi_1}{\partial Z^2}\right|_{Z=0}-\frac{1}{2}f_s^2(X)\left.\frac{\partial^3\psi_0}{\partial Z^3}\right|_{Z=0}-\frac{1}{2}\left(\frac{\mathrm{d}f_s(X)}{\mathrm{d}X}\right)^2\Sigma_s(X) \tag{18}$$

At last, substituting the expressions for each order term $\psi_i(X,Z)$ in Eq. (11) into these identities above, we obtain the coefficients $c_{i,j}$ with the aid of orthogonality of Fourier cosine series, and they are summarized as the following:

$$c_{0,0}=\frac{2}{L_x}\int_0^{L_x/2}\Sigma_s(X)\mathrm{d}X=\frac{2}{L_x}\left(\int_0^{X_p/2}\Sigma_p\mathrm{d}X+\int_{X_p/2}^{L_x/2}\Sigma_f\mathrm{d}X\right)=\frac{X_p}{L_x}(\Sigma_p-\Sigma_f)+\Sigma_f \tag{19}$$

$$c_{0,j}=\frac{4}{(1+4\pi^2j^2/L_x^2)^{1/2}L_x}\int_0^{L_x/2}\Sigma_s(X)\cos\left(\frac{2\pi jX}{L_x}\right)\mathrm{d}X=\frac{4}{(1+4\pi^2j^2/L_x^2)^{1/2}L_x}\left(\int_0^{X_p/2}\Sigma_p\cos\left(\frac{2\pi jX}{L_x}\right)\mathrm{d}X+\int_{X_p/2}^{L_x/2}\Sigma_f\cos\left(\frac{2\pi jX}{L_x}\right)\mathrm{d}X\right)=\frac{2(\Sigma_p-\Sigma_f)\sin(\pi jX_p/L_x)}{(1+4\pi^2j^2/L_x^2)^{1/2}\pi j}\quad j=1,2,3,\ldots \tag{20}$$

$$c_{1,0}=\frac{2}{L_x}\int_0^{X_p/2}\left(-\frac{\mathrm{d}f_p(X)}{\mathrm{d}X}\left.\frac{\partial\psi_0}{\partial X}\right|_{Z=0}+f_p(X)\left.\frac{\partial^2\psi_0}{\partial Z^2}\right|_{Z=0}\right)\mathrm{d}X \tag{21}$$

$$c_{1,j}=\frac{4}{(1+4\pi^2j^2/L_x^2)^{1/2}L_x}\int_0^{X_p/2}\left(-\frac{\mathrm{d}f_p(X)}{\mathrm{d}X}\left.\frac{\partial\psi_0}{\partial X}\right|_{Z=0}+f_p(X)\left.\frac{\partial^2\psi_0}{\partial Z^2}\right|_{Z=0}\right)\cos\left(\frac{2\pi jX}{L_x}\right)\mathrm{d}X\quad j=1,2,3,\ldots \tag{22}$$

$$c_{2,0}=\frac{2}{L_x}\int_0^{X_p/2}\left[-\frac{\mathrm{d}f_p(X)}{\mathrm{d}X}\left.\frac{\partial\psi_1}{\partial X}\right|_{Z=0}-f_p(X)\frac{\mathrm{d}f_p(X)}{\mathrm{d}X}\left.\frac{\partial^2\psi_0}{\partial Z\partial X}\right|_{Z=0}+f_p(X)\left.\frac{\partial^2\psi_1}{\partial Z^2}\right|_{Z=0}+\frac{1}{2}f_p^2(X)\left.\frac{\partial^3\psi_0}{\partial Z^3}\right|_{Z=0}+\frac{1}{2}\left(\frac{\mathrm{d}f_p(X)}{\mathrm{d}X}\right)^2\Sigma_p\right]\mathrm{d}X \tag{23}$$

$$c_{2,j}=\frac{4}{(1+4\pi^2j^2/L_x^2)^{1/2}L_x}\int_0^{X_p/2}\left[-\frac{\mathrm{d}f_p(X)}{\mathrm{d}X}\left.\frac{\partial\psi_1}{\partial X}\right|_{Z=0}-f_p(X)\frac{\mathrm{d}f_p(X)}{\mathrm{d}X}\left.\frac{\partial^2\psi_0}{\partial Z\partial X}\right|_{Z=0}+f_p(X)\left.\frac{\partial^2\psi_1}{\partial Z^2}\right|_{Z=0}+\frac{1}{2}f_p^2(X)\left.\frac{\partial^3\psi_0}{\partial Z^3}\right|_{Z=0}+\frac{1}{2}\left(\frac{\mathrm{d}f_p(X)}{\mathrm{d}X}\right)^2\Sigma_p\right]\cos\left(\frac{2\pi jX}{L_x}\right)\mathrm{d}X\quad j=1,2,3,\ldots \tag{24}$$

And the solution of electrical potential field to the term of second-order could be expressed as

$$\psi(X,Z)\cong\sum_{j=0}^{\infty}c_{0,j}\cos\left(\frac{2\pi jX}{L_x}\right)e^{-(1+4\pi^2j^2/L_x^2)^{1/2}Z}+\varepsilon\sum_{j=0}^{\infty}c_{1,j}\cos\left(\frac{2\pi jX}{L_x}\right)e^{-(1+4\pi^2j^2/L_x^2)^{1/2}Z}+\varepsilon^2\sum_{j=0}^{\infty}c_{2,j}\cos\left(\frac{2\pi jX}{L_x}\right)e^{-(1+4\pi^2j^2/L_x^2)^{1/2}Z} \tag{25}$$

3. Numerical calculation of coefficients $c_{i,j}$

The coefficients of the zero-order term $\psi_0(X,Z)$, $c_{0,j}$, are analytical, as are expressed in Eqs. (19) and (20). In calculation of coefficients of higher-order terms, they will need the knowledge of coefficients of lower-order terms, as is shown through Eqs. (21)–(24). Since $f_s(X)$ (also $\mathrm{d}f_s(X)/\mathrm{d}X$) is zero in the region of flat surface, the upper limit of integration in these integral equations is $X_p/2$. As can be seen from these equations, the derivation of coefficients of higher-order terms is a nontrivial work. There are two possible approaches to this. One approach is expanding both $f_p(X)$ and $\mathrm{d}f_p(X)/\mathrm{d}X$ into their Fourier cosine series, using the derivatives of known lower-order term(s) via direct differentiation term by term from the forms in Eq. (11) at $Z=0$, and calculating the coefficients $c_{i,j}$ by the integration on the right-hand side in these equations. However, this approach is found not applicable. Among the derivatives of lower-order terms via direct differentiation term

by term using the forms in Eq. (11) at $Z=0$, some series might diverge. For example,

$$\left.\frac{\partial\psi_0}{\partial X}\right|_{Z=0} = -\sum_{k=1}^{\infty}\frac{2\pi k c_{0,k}}{L_x}\ \sin\left(\frac{2\pi kX}{L_x}\right) \tag{26}$$

which is convergent from the fact that,

$$\frac{2\pi k c_{0,k}}{L_x} = \frac{4(\Sigma_p-\Sigma_f)\ \sin(\pi kX_p/L_x)}{(1+4\pi^2k^2/L_x^2)^{1/2}L_x} \tag{27}$$

but this derivative,

$$\left.\frac{\partial^3\psi_0}{\partial Z^3}\right|_{Z=0} = -\sum_{k=0}^{\infty}\left(1+\frac{4\pi^2k^2}{L_x^2}\right)^{3/2} c_{0,k}\ \cos\left(\frac{2\pi kX}{L_x}\right) \tag{28}$$

is divergent from the fact that,

$$\left(1+\frac{4\pi^2k^2}{L_x^2}\right)^{3/2} c_{0,k} = \frac{2(1+4\pi^2k^2/L_x^2)(\Sigma_p-\Sigma_f)\sin(\pi kX_p/L_x)}{\pi k} \tag{29}$$

if $\sin(\pi kX_p/L_x)\neq 0$. Another approach, a successful approach, is resorting to both numerical differentiation and numerical integration. The derivatives of known lower-order term(s) at $Z=0$ in the integrands in Eqs. (21)–(24) could be estimated through its (their) measured values using the Newton's central difference (a speedily convergent, second-order method). For some derivatives of known lower-order terms at $Z=0$, the Newton's central difference can be applied directly, including $\left.\partial\psi_i/\partial X\right|_{Z=0}$ and $\left.\partial^2\psi_i/\partial X^2\right|_{Z=0}$, however it cannot be applied directly for the others. These derivatives can be rewritten through some identities for the application of Newton's central difference. For $\left.\partial^2\psi_i/\partial Z^2\right|_{Z=0}$, with the aid of Eq. (10), it can be rewritten by

$$\left.\frac{\partial^2\psi_i}{\partial Z^2}\right|_{Z=0} = -\left.\frac{\partial^2\psi_i}{\partial X^2}\right|_{Z=0} + \psi_i(X,0) \tag{30}$$

For $\left.\partial^2\psi_0/\partial Z\partial X\right|_{Z=0}$, it can be rewritten with the aid of Eq. (16) as

$$\left.\frac{\partial^2\psi_0}{\partial Z\partial X}\right|_{Z=0} = \left.\left(\frac{\partial}{\partial X}\frac{\partial\psi_0}{\partial Z}\right)\right|_{Z=0} = \frac{\mathrm{d}}{\mathrm{d}X}\left(\left.\frac{\partial\psi_0}{\partial Z}\right|_{Z=0}\right) = -\frac{\mathrm{d}\Sigma_s(X)}{\mathrm{d}X} \tag{31}$$

where according to Eq. (3), the last term in this equation is equal to 0 for $X\in[0,X_p/2)$, and therefore this derivative is equal to zero. For $\left.\partial^3\psi_0/\partial Z^3\right|_{Z=0}$, according to Eq. (10), it can be rewritten as

$$\left.\frac{\partial^3\psi_0}{\partial Z^3}\right|_{Z=0} = -\left.\frac{\partial^3\psi_0}{\partial X^2\partial Z}\right|_{Z=0} + \left.\frac{\partial\psi_0}{\partial Z}\right|_{Z=0} \tag{32}$$

where these two terms in the right-hand side can be rewritten via Eq. (16), and this equation above becomes

$$\left.\frac{\partial^3\psi_0}{\partial Z^3}\right|_{Z=0} = \frac{\mathrm{d}^2\Sigma_s(X)}{\mathrm{d}X^2} - \Sigma_s(X) \tag{33}$$

where according to Eq. (3) again, the first and the second terms in the right-hand side are equal to 0 and $-\Sigma_p$ for $X\in[0,X_p/2)$ respectively. At last, substituting the rewritten forms of the derivatives (Eqs. (30) and (33)) into Eqs. (21)–(24), and using the Newton's central difference, together with the expressions of both $f_p(X)$ and $\mathrm{d}f_p(X)/\mathrm{d}X$, we thus obtain the undetermined coefficients $c_{i,j}$ via the numerical integration.

4. Results and discussion

In evaluating the electrical potential field, the asymptote expansion series, expressed in Eq. (9), could be expanded to a higher-order term if needed, and the derivation for higher-order terms is quite similar to that of lower-order terms, but numerical calculation will be more laborious. In our present calculation, we expand it to the second-order term, as is shown in Eq. (25), for the accuracy by Eq. (25) is high enough for the values of ε used in present calculation (up to 0.1 ultimately). The number of terms in each eigenfunction expansion series for each order term, shown in Eq. (11), is taken as 50 initially, doubled in the succeeding iteration, and iteration is stopped when the values of each order term of ψ in two successive iterations are different from each other by a tolerance less than 1×10^{-4}. Numerical calculations show that, the number of terms in the eigenfunction expansion series of each order term needed is 400 at the utmost. For illustration of the suggested methodology, a polynomial form for the shape function of protrusion is chosen, which can be expressed as

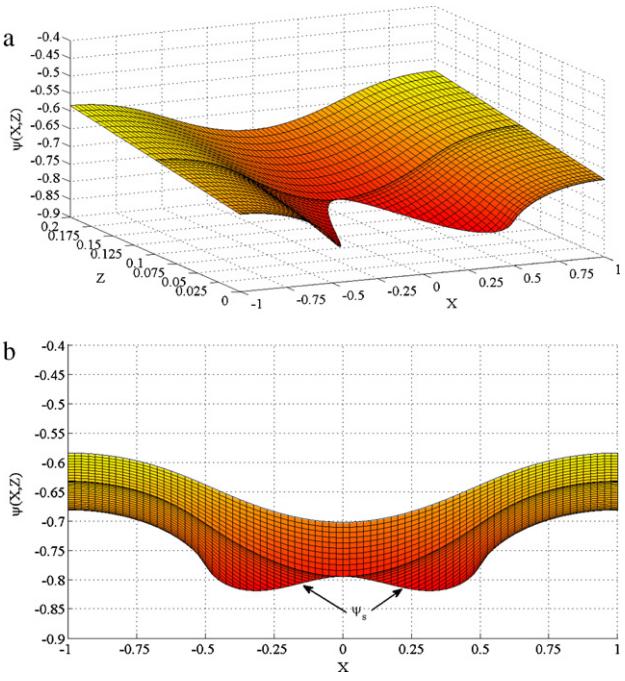

Fig. 2. (a) The solution surface of $\psi(X,Z)$ on X–Z plane. (b) The lateral view of $\psi(X,Z)$ along the direction parallel to Z axis, where the surface electrical potential ψ_s is also shown in this figure. $L_x=2$, $\varepsilon=0.1$, $\Sigma_p=-1$.

$$f_p(X) = 16\left|\frac{X}{X_p}\right|^3 - 12\left(\frac{X}{X_p}\right)^2 + 1 \tag{34}$$

This polynomial shape function has its values equal to 1 and 0 at $X=0$ and $X=\pm X_p/2$, respectively, and also has its derivative equal to zero at these points. In addition, it is symmetric about the Z axis. Moreover, $X_p=1$, and $\Sigma_f=-0.5$. The dimensionless form of surface charge density $\Sigma_s(X)$ (or Σ_p and Σ_f) has its physical meaning. When a flat, uniformly charged surface is under consideration, it is equal to the value of ψ on surface. Therefore, for applicability of Debye–Huckel approximation, its value is confined to 1 at the utmost in our analysis. Fig. 2 demonstrates the numerical result of electrical potential field for our charged surface system when $L_x=2$, $\varepsilon=0.1$, and $\Sigma_p=-1$. In this figure, to display the surface electrical potential on protrusion, we have made the grids of X axis (meridians) equally spaced, and the grids of Z axis (parallels) spaced according to the intersections between the grids of X and the surface of protrusion in the region lower than the vertex of protrusion. The electrical potential field of our charged surface system is symmetric about three planes, including $X=0$, and $X=\pm L_x/2$. From the solution surface of $\psi(X,Z)$ shown in Fig. 2(a), the electrical potential field appears mainly a strong function of X in both the regions above and below the vertex of protrusion, and in the meanwhile,

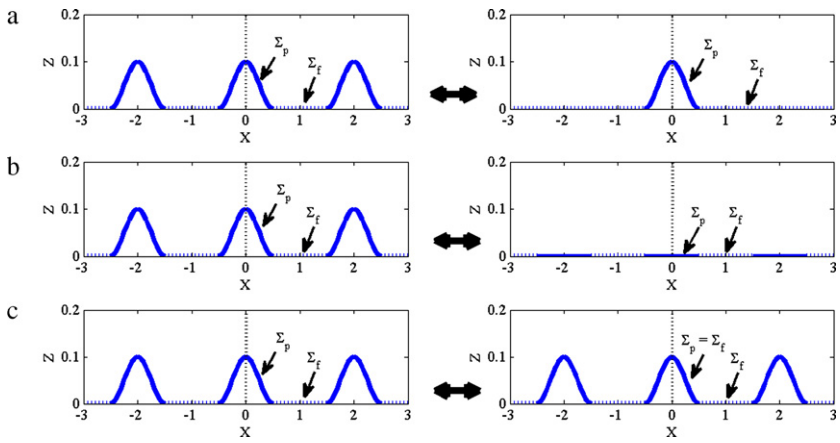

Fig. 3. Comparison with three special conditions, including (a) an isolated dissimilarly charged protrusion, (b) the dissimilarly charged flat surfaces, and (c) the similarly charged protrusions. The solid curves, the solid lines, and the dot lines denote the protrusions, the dissimilarly charged flat surfaces, and the flat surfaces, respectively.

it shows a depression near the protrusion, wherein the lowest of depression seems to be near the interface between the protrusion and the flat surface ($X = \pm X_p/2$). To understand the distribution of electrical potential field in a more detailed manner, we depict the lateral view of $\psi(X, Z)$ along the direction parallel to Z axis, together with the surface electrical potential $\psi_s(X)$ of charged surface system (a function of X), as is illustrated in Fig. 2(b). Along each meridian from the charged surface (going deeper into the electrolyte solution), the magnitude of ψ decreases; along each parallel from $X = \pm L_x/2$, the magnitude of ψ increases, and it reaches to a maximum on the surface of protrusion (or at $X = 0$). The latter reveals the fact that the surface charge density on protrusion surface is greater than that of on flat surface in magnitude, i.e. $|\Sigma_f| < |\Sigma_p|$. The surface electrical potential ψ_s shows a more interesting distribution. The magnitude of ψ_s increases for a start from $X = \pm L_x/2$, reaches to a maximum near $X = \pm X_p/2$, and decreases gradually to a minimum at the vertex of protrusion, wherein the minimum is far higher than its magnitude at $X = \pm L_x/2$. There are two effects in the main which are responsible for this. One is the strength of charges on charged surface system, and the other is the concavity of surface, wherein the latter has been discussed in a previous work [18], and the analysis from this work shows that the concave inward/outward on a charged surface will strengthen/weaken the magnitude of electrical potential field. Basically, the magnitude of ψ_s on protrusion surface is presumably greater than that on flat surface, since $|\Sigma_f| < |\Sigma_p|$. However, these two concavities near the vertex of protrusion ($X = 0$) and near the interface between the protrusion and the flat surface ($X = \pm X_p/2$), where they are respectively concave outward and inward (referring to Fig. 1(b)), would weaken and strengthen the magnitude of ψ_s respectively. As a consequence, considering both of these two effects, i.e. the strength of charges on charged surface system and the concavity of surface, the surface electrical potential ψ_s appears an interesting profile shown in this figure. These two effects are also responsible for the behavior of electrical potential field in the region near the charged surface.

The purpose of present work is mainly the presentation of both the suggested charged surface model and the methodology introduced, however, there are some important subjects worthy of discussion here. Fig. 3 illustrates these subjects under consideration. In the first subject, we discuss the condition of an isolated dissimilarly charged protrusion (referring to Fig. 3(a)), which is quite useful when we concern the electrostatic phenomenon of a local protrusion. The suggested charged surface model could easily simulate this condition. When the period of charged surface system L_x is extended to a quite large value, EDL configuration approaches to that in this condition. Fig. 4(a) and (b) demonstrate respectively the solution surface and the lateral view of $\psi(X, Z)$ along the direction parallel to Z axis when $L_x = 4$, $\varepsilon = 0.1$, and $\Sigma_p = -1$. Compared with Fig. 2 it is found that, when the period of charged surface system is increased, the distance between two neighbor protrusions also increases, and correspondingly, the effect from the charges on protrusions become weaker. Therefore, the magnitude of ψ decreases as a whole. From the parallels shown in Fig. 4(b), it is also found that, when the protrusion is isolated, the dependence of ψ on X becomes stronger, due to the isolation of protrusion. Although the electrical potential field becomes weaker in its magnitude, its behavior is quite similar to that in Fig. 2, including the surface electrical potential ψ_s. The second subject discusses the effect of protrusion. To do this, we calculate $\psi(X, Z)$ in the condition of dissimilarly charged flat surfaces, and that is that when $\varepsilon = 0$ (referring to Fig. 3(b)). The electrical potential field in this condition

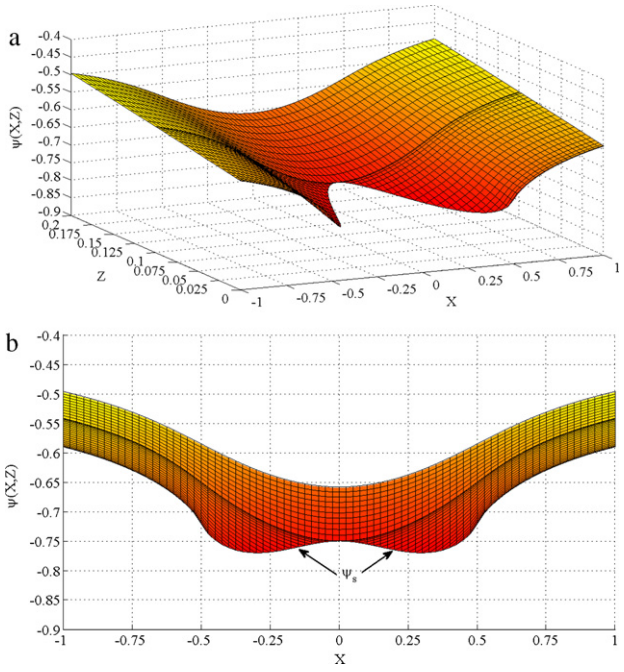

Fig. 4. (a) The solution surface of $\psi(X, Z)$ on X–Z plane. (b) The lateral view of $\psi(X, Z)$ along the direction parallel to Z axis, where the surface electrical potential ψ_s is also shown in this figure. $L_x = 4$, $\varepsilon = 0.1$, $\Sigma_p = -1$.

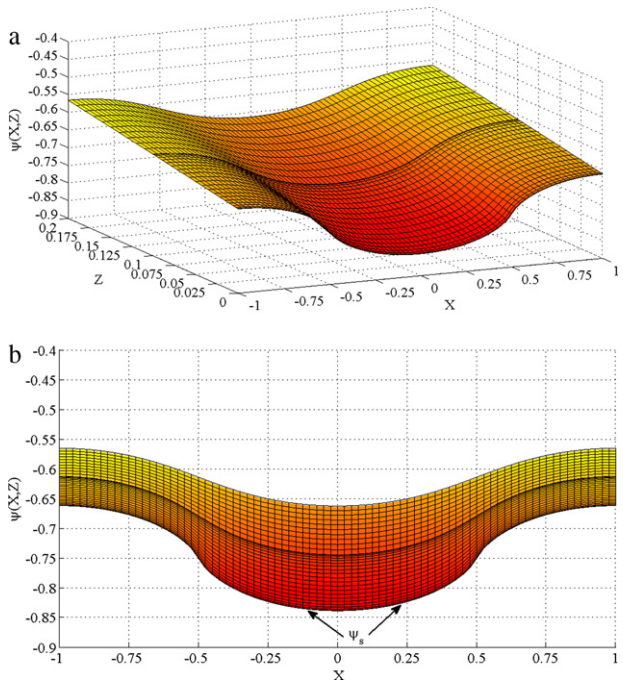

Fig. 5. (a) The solution surface of $\psi(X, Z)$ on X–Z plane. (b) The lateral view of $\psi(X, Z)$ along the direction parallel to Z axis, where the surface electrical potential ψ_s is also shown in this figure. $L_x = 2$, $\varepsilon = 0$, $\Sigma_p = -1$.

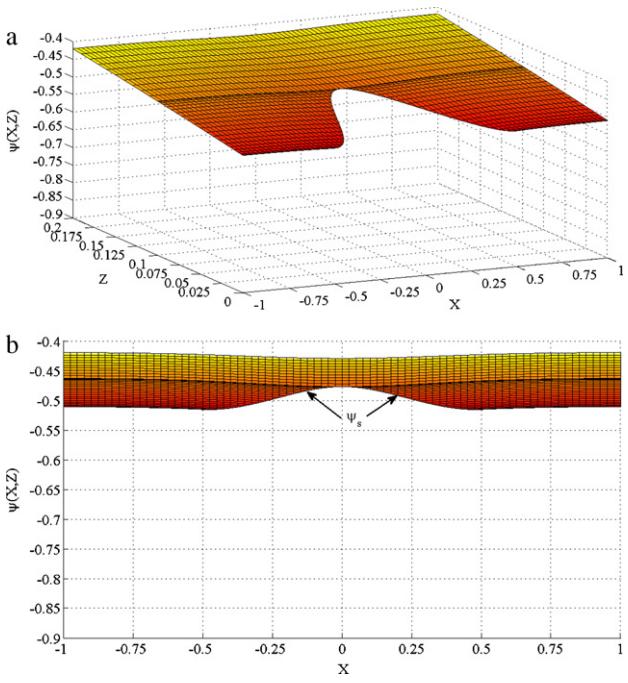

Fig. 6. (a) The solution surface of $\psi(X, Z)$ on X–Z plane. (b) The lateral view of $\psi(X, Z)$ along the direction parallel to Z axis, where the surface electrical potential ψ_s is also shown in this figure. $L_x = 2$, $\varepsilon = 0.1$, $\Sigma_p = \Sigma_f = -0.5$.

is the zero-order term in (25), or in mathematical expression:

$$\psi_0(X,Z) = \left[\frac{X_p}{L_x}(\Sigma_p - \Sigma_f) + \Sigma_f\right] e^{-Z} + \sum_{j=1}^{\infty} \frac{2(\Sigma_p - \Sigma_f)\sin(\pi j X_p/L_x)}{(1 + 4\pi^2 j^2/L_x^2)^{1/2}\pi j} \cos\left(\frac{2\pi j X}{L_x}\right) e^{-(1+4\pi^2 j^2/L_x^2)^{1/2} Z} \quad (35)$$

The solution surface and the lateral view of $\psi(X, Z)$ along the direction parallel to Z axis when $L_x = 2$, $\varepsilon = 0$, and $\Sigma_p = -1$ are illustrated in Fig. 5(a) and (b) respectively. Compared with Fig. 2, it is found surprisingly that, the electrical potential field does not seem to be affected significantly by the presence of protrusion, except that its magnitude is strengthened slightly. The parallels at each level of Z shown in Fig. 5(b) are quite similar to those in Fig. 2(b). This can be realized if we consider the concavity of protrusion surface mentioned above. When the protrusion surface protrudes into the electrolyte solution, it is likely to increase the magnitude of electrical potential field nearby. However in the meantime, the concave outward of protrusion will reduce the effect of charges on protrusion surface. As a consequence, these two effects offset each other, and $\psi(X, Z)$ remains unchanged almost. For the condition of dissimilarly charged flat surfaces, since the dissimilarly charged surfaces do not protrude into the electrolyte solution, from $X = \pm L_x/2$, the magnitude of ψ_s increases gradually, and reaches to a maximum at $X = 0$, as is shown in Fig. 5(b). The last subject discusses the effect of dissimilarly charged condition on protrusions (referring to Fig. 3(c)). To understand this effect, we set the surface charge density on protrusions being the same with that on flat surface (similarly charged protrusions), i.e. $\Sigma_p = \Sigma_f$, and the solution surface and the lateral view of $\psi(X, Z)$ along the direction parallel to Z axis are depicted in Fig. 6(a) and (b) respectively, where in these two figures, $L_x = 2$, $\varepsilon = 0.1$, and $\Sigma_p = \Sigma_f = -0.5$. Compared with Fig. 2, we find that, dissimilarly charged condition could lead to large change of electrical potential field, in both its magnitude and its distribution. For condition of similarly charged protrusions, for the same reason mentioned above that, two effects, including the depth into the electrolyte solution for the protrusion, and the concave outward of protrusion, offset each other, the distribution of $\psi(X, Z)$ is quite similar to that for the condition of completely flat surface carrying uniform charges with its surface charge density Σ_f. Consequently, if we consider the discussion in the second subject, it can be concluded that, the effect of dissimilarly charged condition on EDL configuration is nearly independent of the geography of charged surface system.

In present work, for illustration, we designate the shape function of protrusion as a polynomial form, and the surface charge density of both protrusion and flat surface as a constant. However, this condition is just a special one that the methodology suggested here could deal with. According to Eqs. (19)–(24), derivation of coefficients $c_{i,j}$ needs only the knowledge of both the shape function of protrusion and the form of surface charge density on our charged surface system. Therefore, this suggested model can be applied on any form of shape function of protrusion (even the shape function has jumps), for example, the rectangular, the indentation (protrusion downward), the triangular, the circular (referring to Fig. 7), and so forth. In the meanwhile, it is also applicable for any form of charged condition on charged surface system, not confined to the condition of step form in our illustration, as is shown in Fig. 1(c). In addition to these above, the applicability of present charged surface model is not confined to the condition of symmetry geometry. In the demonstration in present work, the symmetry geometry is introduced for solely mathematical simplicity, and based on such an assumption, only the cosine-form eigenfunctions in Eq. (11) need to be considered. When a condition of asymmetric geometry is under consideration, the sine-form eigenfunctions should be also taken into account in Eq. (11). Nevertheless, this solely raises the calculation work, and does not raise the complexity of computing algorithm used. For conceptual presentation, the suggested methodology is here illustrated on a one-dimensional charged surface, however, it can be extended directly to a more general, more realistic, two-dimensional charged surface, and this will be a focal point in our oncoming work.

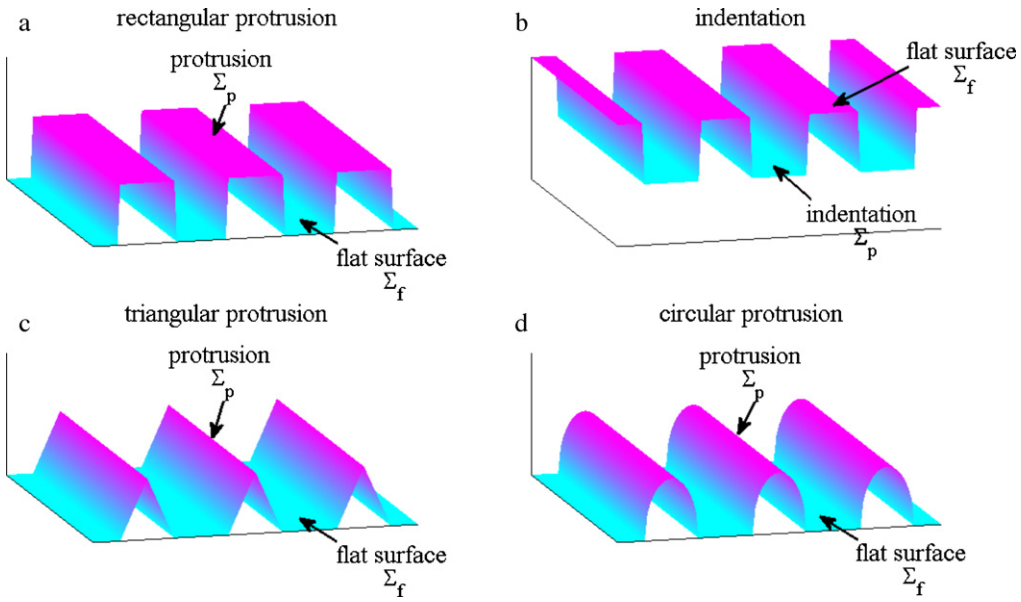

Fig. 7. Illustration for the variant of protrusions, including (a) the rectangular, (b) the indentation, (c) the triangular, and (d) the circular.

5. Conclusions

In this work, combining both the conditions of dissimilarly charged flat surfaces and similarly charged protrusions, we successfully derive the semi-analytical solution for EDL configuration near a dissimilarly charged surface model, a model simulating simultaneously both arbitrary surface geography and surface charged condition. The coefficients in eigenfunction expansions for the solution are estimated accurately via both numerical difference and numerical integration. Some important conclusions from the analysis could be summarized as follow:

(1) When the period of charged surface system increases, the electrical potential field becomes a more stronger function of abscissa, however its magnitude gets smaller.
(2) The electrical potential field does not be affected significantly by the presence of protrusions.
(3) Dissimilarly charged condition would affect largely the electrical potential field in both its magnitude and its distribution, and also, its effect is nearly independent of the geography of charged surface system.

Acknowledgment

This work is supported by the National Science Council of the Republic of China under grant NSC 97-2221-E-197-013-MY3.

References

[1] P. Sweeney, T. Karashima, H. Ishikura, S. Wiehle, M. Yamashita, W.F. Benedict, R.J. Cristiano, C.P.N. Dinney, Efficient therapeutic gene delivery after systemic administration of a novel polyethylenimine/DNA vector in an orthotopic bladder cancer model, Cancer Res. 63 (2003) 4017–4020.
[2] Y.C. Kuo, K.H. Shih, J.T. Yang, Capillary electrophoresis of bone marrow stromal cells with uptake of heparin-functionalized poly(lactide-co-glycolide) nanoparticles during differentiation towards neurons, Electrophoresis 31 (2010) 315–323.
[3] J.J. Heikkinen, J.P. Heiskanen, O.E.O. Hormi, Grafting of functionalized silica particles with poly(acrylic acid), Polym. Adv. Technol. 17 (2006) 426–429.
[4] J.W. Kim, L.U. Kim, C.K. Kim, Size control of silica nanoparticles and their surface treatment for fabrication of dental nanocomposites, Biomacromolecules 8 (2007) 215–222.
[5] P. Yin, Q. Xu, R. Qu, G. Zhao, Y. Sun, Adsorption of transition metal ions from aqueous solutions onto a novel silica gel matrix inorganic-organic composite material, J. Hazard. Mater. 173 (2010) 710–716.
[6] R.C. Bohinski, Modern Concepts in Biochemistry, 5th ed., Allyn and Bacon Inc., 1987.
[7] G. Guidotti, Membrane proteins, Annu. Rev. Biochem. 41 (1972) 731–752.
[8] G.V.F. Seaman, D.H. Heard, Methods: a microelectrophoresis chamber of small volume for use with biological systems, Blood 18 (1961) 599–604.
[9] G.V.F. Seaman, G. Uhlenbruck, The surface structure of erythrocytes from some animal sources, Arch. Biochem. Biophys. 100 (1963) 493–502.
[10] D.A. Haydon, G.V.F. Seaman, Electrokinetic studies on the ultrastructure of the human erythrocyte: i. electrophoresis at high ionic strengths – the cell as a polyanion, Arch. Biochem. Biophys. 122 (1967) 126–136.
[11] T.R. Weikl, M.M. Kozlov, W. Helfrich, Interaction of conical membrane inclusions: effect of lateral tension, Phys. Rev. E 57 (1998) 6988–6995.
[12] H. Ohshima, Electrophoresis of soft particles, Adv. Colloid Interface Sci. 62 (1995) 189–235.
[13] J.P. Hsu, S.H. Lin, S. Tseng, Effect of cell membrane structure of human erythrocyte on its electrophoresis, Colloids Surf. B 32 (2003) 203–212.
[14] L. Suresh, J.Y. Walz, Effect of surface roughness on the interaction energy between a colloidal sphere and a flat plate, J. Colloid Interface Sci. 183 (1996) 199–213.
[15] A. Fogden, D.J. Mitchell, B.W. Ninham, Undulations of charged membranes, Langmuir 6 (1990) 159–162.
[16] A. Fogden, B.W. Ninham, The bending modulus of ionic lamellar phases, Langmuir 7 (1991) 590–595.
[17] M. Kostoglou, A.J. Karabelas, Effect of roughness on energy of repulsion between colloidal surfaces, J. Colloid Interface Sci. 171 (1995) 187–199.
[18] S.H. Lin, Charged layer with undulated surface: configuration of electrical double layer, Colloids Surf. B 78 (2010) 127–139.
[19] S.H. Lin, Electrokinetic flow near an undulated, charged surface, Colloids Surf. B 81 (2010) 224–234.